Coseismic deformation of the Mid Niigata prefecture Earthquake in 2004 detected by RADARSAT/InSAR

Taku Ozawa, Sou Nishimura, Yutaka Wada, and Hiroshi Ohkura

National Research Institute for Earth Science and Disaster Prevention, Japan

(Received February 11, 2005; Revised April 15, 2005; Accepted April 18, 2005)

Crustal deformation associated with the Mid Niigata prefecture Earthquake in 2004 ($M_{JMA} = 6.8$) was detected using RADARSAT SAR interferometry. A displacement of -40 cm in the line-of-sight to the satellite was observed to the west of the main shock epicenter, and a displacement of 20 cm was observed to the east of the epicenter. Fault parameters estimated from the obtained deformation were in good agreement with those of the Centroid Moment Tensor solution for the main shock provided by the Japan Meteorological Agency. In the postseismic period, a steep gradient of deformation was found around the Obiro and the Western Muikamachi Basin faults, indicating that a fault-slip occurred in the shallow part of the fault. Since the seismicity in the shallow part of the Western Muikamachi Basin fault was very low, we believe that it must have been an aseismic slip. Crustal deformation associated with an aftershock that occurred on October 27 ($M_{JMA} = 6.1$) was detected, and it was ascertained that this aftershock had ruptured the conjugate plane with respect to the Obiro fault. Since locations and/or mechanisms of these faults differed significantly, it was determined that at least three faults were involved in this series of earthquakes.

Key words: InSAR, mid-Niigata Earthquake, coseismic, postseismic, crustal deformation.

1. Introduction

The Mid Niigata prefecture Earthquake in 2004 ($M_{JMA} = 6.8$) occurred in northeastern Japan at 8:56 (GMT: Greenwich Mean Time) on October 24. According to the Japan Meteorological Agency (JMA), the hypocenter of this earthquake was located at 37.239°N latitude, 138.870°E longitude at a depth of 13.1 km (Fig. 1), and the focal mechanism was a reverse-fault type. The largest aftershock ($M_{JMA} = 6.5$) occurred at 9:34 on the same day (Fig. 1), and its focal mechanism was also a reverse-fault type. Including these, earthquakes larger than M6.0 occurred four times on October 23 and once on October 27. The Japanese nationwide GPS network (GEONET) observed crustal deformation associated with these earthquakes. The obtained displacement field and the estimated fault mechanism, which is a reverse-fault type, were published (Imakiire, 2005). GPS results and the aftershock distribution suggested that several fault planes had been ruptured in this series of earthquakes. For example, the largest aftershock ruptured the parallel plane to the main shock fault, and the aftershock that occurred on October 27 ruptured the conjugate plane (e.g., Hirata *et al.*, 2005; Kato *et al.*, 2005; Sakai *et al.*, 2005; Shibutani *et al.*, 2005). To investigate such a complex fault mechanism, more spatially detailed deformation data is useful, thus we applied a synthetic aperture radar interferometry (InSAR) technique around the epicentral area. In this paper, we present the obtained deformation field in the coseismic and postseismic periods and discuss faults that are related to this series of earthquakes.

2. SAR Data and InSAR Pairs

The RADARSAT satellite was able to observe the epicentral area at 20:45 (GMT) on October 24, which was the earliest SAR observation after the main shock. Therefore we selected RADARSAT SAR for this analysis and requested an observation on October 24. The observation mode was "F1N"; the incidence angle was 38°, the swath width was 50 km and the pixel size was 5 m. InSAR can detect one component of displacement, projecting the ground displacement vector onto the line-of-sight (LOS) of the radar. The LOS direction for this data was (-0.602, 0.111, -0.790) in the coordinate set (east, north, up). Each fringe of the RADARSAT interferogram represents LOS displacement of 2.85 cm, half of the wavelength of the radar.

In this study, we analyzed two interferometric pairs to detect crustal deformation that occurred during the coseismic and postseismic periods. First, an interferogram was generated using SAR data acquired from a descending orbit on September 30 and October 24 (Pair 1). In this period, the main shock, the largest aftershock, and two other aftershocks larger than M6.0 occurred. The interferogram of Pair 1 thus represents the sum of crustal deformation caused by these earthquakes and/or by postseismic deformation that must have occurred within 1.5 days. A second interferogram was generated using SAR data acquired from a descending orbit on October 24 and November 17 (Pair 2). During this period, an M6.1 aftershock occurred on October 27. The interferogram of Pair 2 represents the sum of crustal deformation caused by this aftershock and/or post-

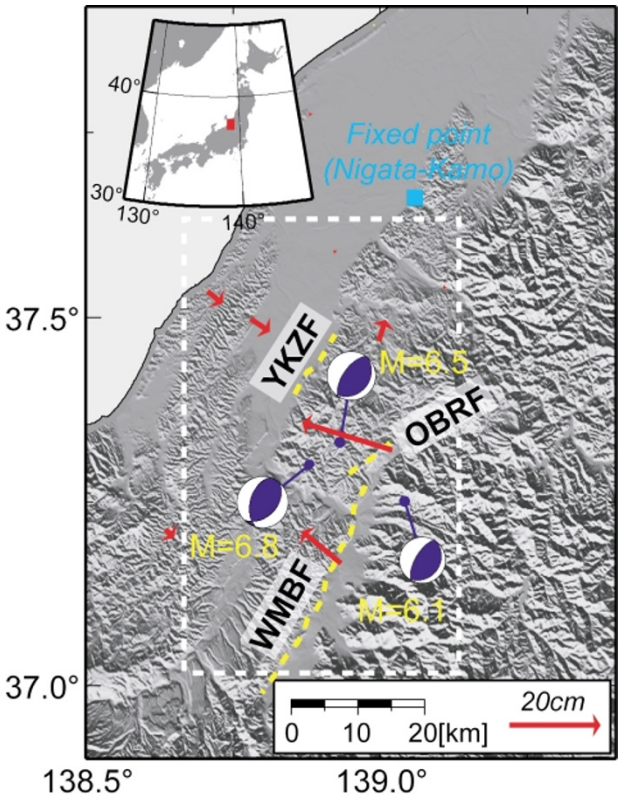

Fig. 1. Shaded-relief topographic map of the epicentral area. Blue circles associated with the focal mechanism denote epicenters of the main shock (M6.8), the largest aftershock (M6.5), and the aftershock on October 27 (M6.1), provided by JMA. Red arrows indicate displacements that occurred during the period corresponding to Pair 1 observed by GEONET. Dashed yellow lines indicate the Obiro (OBRF), the Western Muikamachi Basin (WMBF), and the Yukyuzan (YKZF) faults. The dashed white box corresponds to the area illustrated in Figs. 2 and 3. The blue square indicates the fixed point for displacement fields of InSAR and GPS. The inset exhibits the area of this figure.

seismic deformation that must have occurred after October 24.

3. Pair 1: Crustal Deformation in the Coseismic Period

3.1 Interferogram and displacement field

The orbit difference (baseline) of Pair 1 is 900 m (the perpendicular component with respect to LOS is 770 m). Good coherence was obtained in and around populated and flat areas where vegetation is scarce (Fig. 2), although baseline condition was never suitable for the application to InSAR. Several GEONET stations have been operating in the area where coherence was obtained, and we compared displacements in LOS obtained by InSAR with those calculated from three-dimensional displacement vectors observed by GEONET (Table 1). These were in good agreement within 3 cm, indicating that the obtained displacement field has an accuracy of several centimeters.

Interferometric fringes around Ojiya City, located to the west of the epicenter, reveal that the ground moved toward the satellite. The largest displacement detected from InSAR, −40 cm, was observed in this area (Fig. 2). We suspect that displacement around the epicenter was even larger, but coherence could not be obtained. In contrast, interferometric fringes around Uonuma City, located to the east of the epicenter, reveal that the ground moved away from the satellite. At the center of this deformation, a displacement of 20 cm was observed by InSAR.

As mentioned above, the obtained deformation reveals that the western area of the epicenter moved toward the satellite and that the eastern area moved away from the satellite. Such a deformation pattern roughly corresponds to crustal deformation induced by reverse faulting, which thrusts the west area over the east area.

3.2 Estimation of fault parameters

To estimate the configuration of the main shock fault, we assumed that the obtained displacement field could be explained by a rectangular fault, and estimated parameters for the elastic half-space dislocation model (Okada, 1985) using a grid-search algorithm. Although InSAR provides displacement data for about 100,000 points, it is inefficient to use all data points for the inversion analysis. We applied the Quadtree algorithm (Samet and Webber, 1988), and reduced the input data to 153 points.

The interferogram simulated using estimated parameters explains the observed data well (Fig. 2(b)), and the root-mean squared residual (RMS) is 9 mm. To evaluate the stability of the estimated parameters, we calculated a range in which the RMS reached 18 mm (twice its minimum; value in parentheses in Table 2). It illustrates that the location and geometry of the fault were constrained particularly well. Estimated parameters are in good agreement with the Centroid Moment Tensor (CMT) solution from JMA with respect to the strike, dip, and rake directions, as well as the moment magnitude (Table 2). Although the location of the fault was estimated in several kilometers west from that of the CMT, such difference was also obtained from the relocation analysis of hypocenters, suggesting that it had been caused by the heterogeneity of the crustal structure (Sakai *et al.*, 2005; Shibutani *et al.*, 2005). These parameters may be not necessarily consistent, but we believe from this agreement that estimated parameters represent the fault configuration of the main shock well.

The estimated fault is located between the Obiro and the Yukyuzan faults where there are no Quaternary active faults, rather it seems that the line where the extension of the fault intersects the surface (thick dashed red line in Fig. 2(b)) corresponds to the Kajikane syncline axis that

Table 1. Comparison between InSAR and GPS displacements in LOS.

Station No.	Sep. 30–Oct. 24		Oct. 24–Nov. 17	
	InSAR	GPS	InSAR	GPS
970810	−9	-9	5	-2
020961	0	6	3	8
970807	−21	−28	2	−1
960568	141	168	−17	−16
950242	59	73	18	10
970806	−8	−5	8	−3
950246	−2	4	5	3

unit: mm

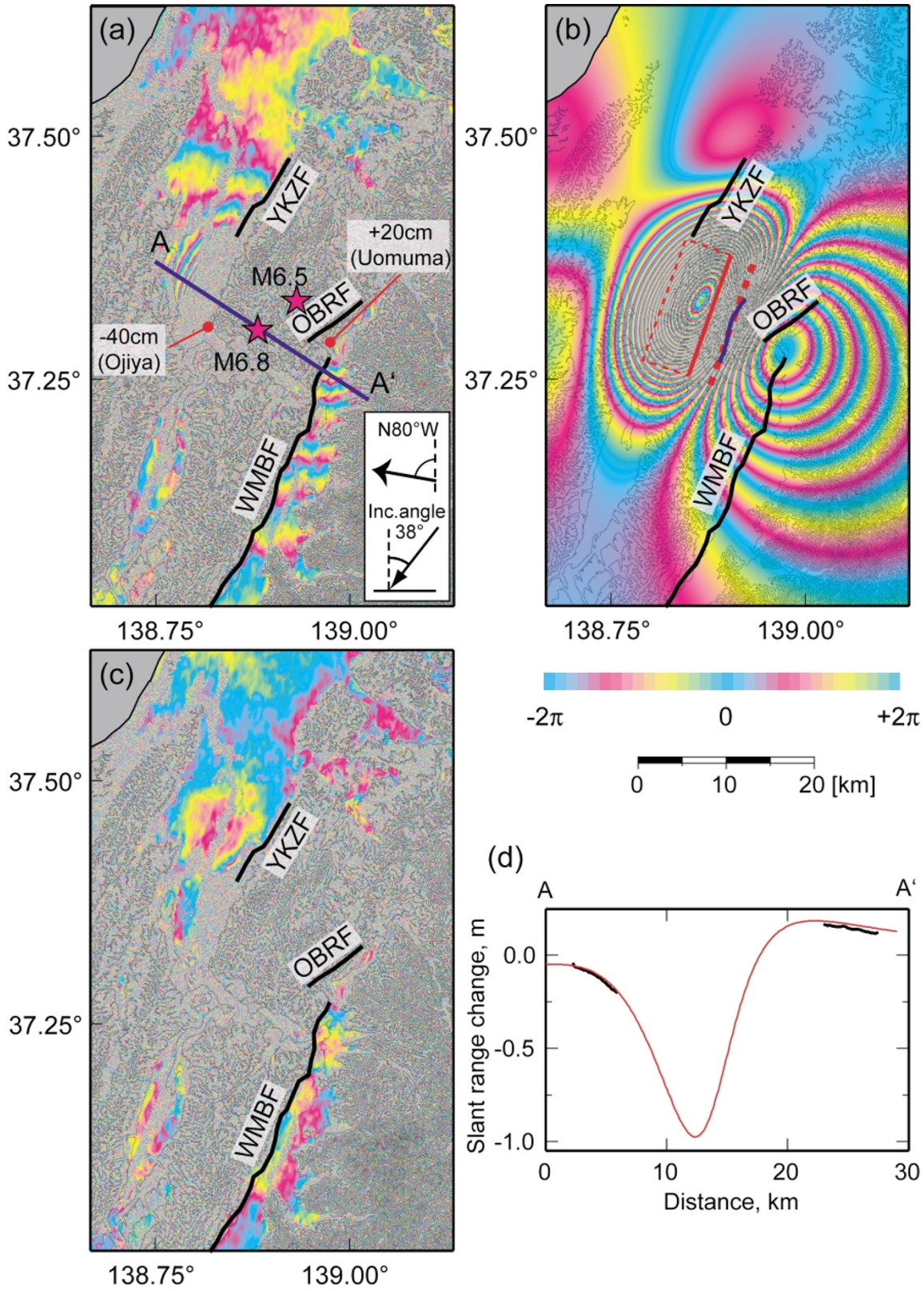

Fig. 2. (a) Interferogram generated from SAR data acquired on September 30 and October 24. Thick solid lines represent the Yukyuzan (YKZF), the Obiro (OBRF), and the Western Muikamachi Basin faults (WMBF). Purple stars denote epicenters of the main shock (M6.8) and the largest aftershock (M6.5). Thin contours represent the topographic height every 100 m. The blue line corresponds to the profile AA′ illustrated in Fig. 2(d). The inset indicates the observation geometry of InSAR. (b) Simulated interferogram. The dashed red rectangle indicates the location of the estimated fault. The red line on the rectangle denotes its upper edge. The thick dashed red line indicates the location where an extension of the fault intersects the surface. The blue curve indicates the location of the Kajikane syncline axis. (c) Residual interferogram (observation–simulation). (d) Displacement profile along AA′ of Fig. 2(a). Solid and red curves indicate observed and simulated displacements.

Table 2. Comparison between estimated parameters and CMT solution from JMA.

	Latitude (°)	Longitude (°)	Depth (km)	Strike (°)	Dip (°)	Rake (°)	Length (km)	Width (km)	Slip (m)	M_W
This study*2	37.335*1	138.818*1	9.4*1	200	45	72	14.6	7.7	3.89	6.8
	(0.009)	(0.010)	(1.3)	(12)	(3)	(16)	(3.0)	(1.0)	(0.61)	
JMA CMT	37.300	138.880	12.1	197	51	73				6.7

*1 Indicates the location of the lower center of the fault.

*2 Values in parentheses are a range of which the RMS reaches 18 mm (twice its minimum).

was mapped on the geological map (blue line in Fig. 2(b); Yanagisawa *et al.*, 1986). Conceivably, the occurrence mechanism of the main shock might relate to such a structure of a fold.

This result does not necessarily indicate that the fault slip did not occur on other faults. Indeed, a systematic residual appears around the Western Muikamachi Basin fault (Fig. 2(c)), possibly caused by a discrepancy in the assumption that the displacement field can be explained by a single fault. Therefore, a small error may be included in estimated parameters, but it need not affect this discussion. To investigate whether the rupture occurred on other faults, additional data and a more detailed analysis will be required.

4. Pair 2: Crustal Deformation in the Postseismic Period

4.1 Interferogram and displacement field

The baseline of Pair 2 was 180 m (the perpendicular component was 170 m), and good coherence was obtained in a populated areas and also in a mountain area (Fig. 3). A comparison between the displacements in LOS observed by InSAR and those calculated from GEONET displacement vectors exhibits good agreement within 11 mm (Table 1), indicating that the obtained displacement field has the same or better accuracy than that of Pair 1. It may have been due to much better coherence than that of Pair 1. A displacement indicating that the ground moved toward the satellite was found in the epicentral area of 20×30 km. The largest displacement, -8 cm, was observed to the west of the Obiro fault (Fig. 3).

4.2 Crustal deformation around the Western Muikamachi Basin fault

A discontinuity in the interferometric fringe appeared for 20 km along the Western Muikamachi Basin fault (solid line of Fig. 3(a)). The displacement profile BB′ illustrates that displacement across the fault is 5 cm in LOS component (Fig. 3(b)). Actually, flexural deformation of 10 to 20 cm was found in one part of the fault in a survey conducted by Nagoya University (Suzuki *et al.*, 2004), supporting our results.

This deformation indicates that the western area of the fault moved toward the satellite. It is possible that landslides occurred in this area corresponding to a mountain area. However, a fringe pattern caused by landslides would be more complex and more local, relating to the topography. Therefore, we think that this possibility is unlikely. In contrast, the obtained deformation reveals the eastern area moved away from the satellite. It is possible that land subsidence occurred in this area corresponding to a basin area. Although this possibility cannot be completely rejected, we believe that the interpretation that this deformation was caused by a faulting is reasonable because it would explain deformation in both sides of the fault. We then tried to account for the displacement profile BB′ with forward iteration of the elastic half-space dislocation model (Okada, 1985). Fault A in Table 3 shows the estimated parameter that was obtained from this analysis. Although this is a preliminary result, the simulated displacement from it agrees with the observed one (red line in Fig. 3(b)). In this estimation, the rake, strike, and length of the fault were fixed parameters, which were supposed from the interferogram. The upper edge of the fault is consistent with the Western Muikamachi Basin fault. Furthermore the dip angle is also similar to that of the Western Muikamachi Basin fault (Yanagisawa *et al.*, 1986). These facts indicate that the Western Muikamachi Basin fault was involved in this series of earthquakes.

The bottom edge of the fault was also fixed to a depth of 5 km in this estimation because it was not constrained uniquely. Therefore, we cannot decide if the fault slip occurred in the deeper part of the fault. However, if the upper edge of the fault was not very shallow, this steep gradient of the displacement cannot be explained. It indicates that the fault slip occurred in the shallow part of the Western Muikamachi Basin fault. However, few aftershocks occurred in the shallow part around the area (Fig. 3(d)). This indicates the possibility that an aseismic slip occurred in the shallow part of the Western Muikamachi Basin fault during the postseismic period.

4.3 Crustal deformation associated with the aftershock on October 27

A steep gradient of deformation was also observed for 5 km along the Obiro fault, extending to the north from the Western Muikamachi Basin fault. Its deformation illustrates that the western area of the fault moved toward the satellite relative to the eastern area (Fig. 3(c)). Near the Obiro fault, it was reported that a surface rupture with a gap of 10 to 20 cm appeared (Maruyama *et al.*, 2005), which is consistent with our result. It seems to indicate that a fault slip also occurred in the shallow part of the Obiro fault. However, both sides of the fault moved toward the satellite. Such a deformation pattern cannot be explained by a single reverse fault. This implies that the crustal deformation associated with the aftershock that occurred to the east of the fault on October

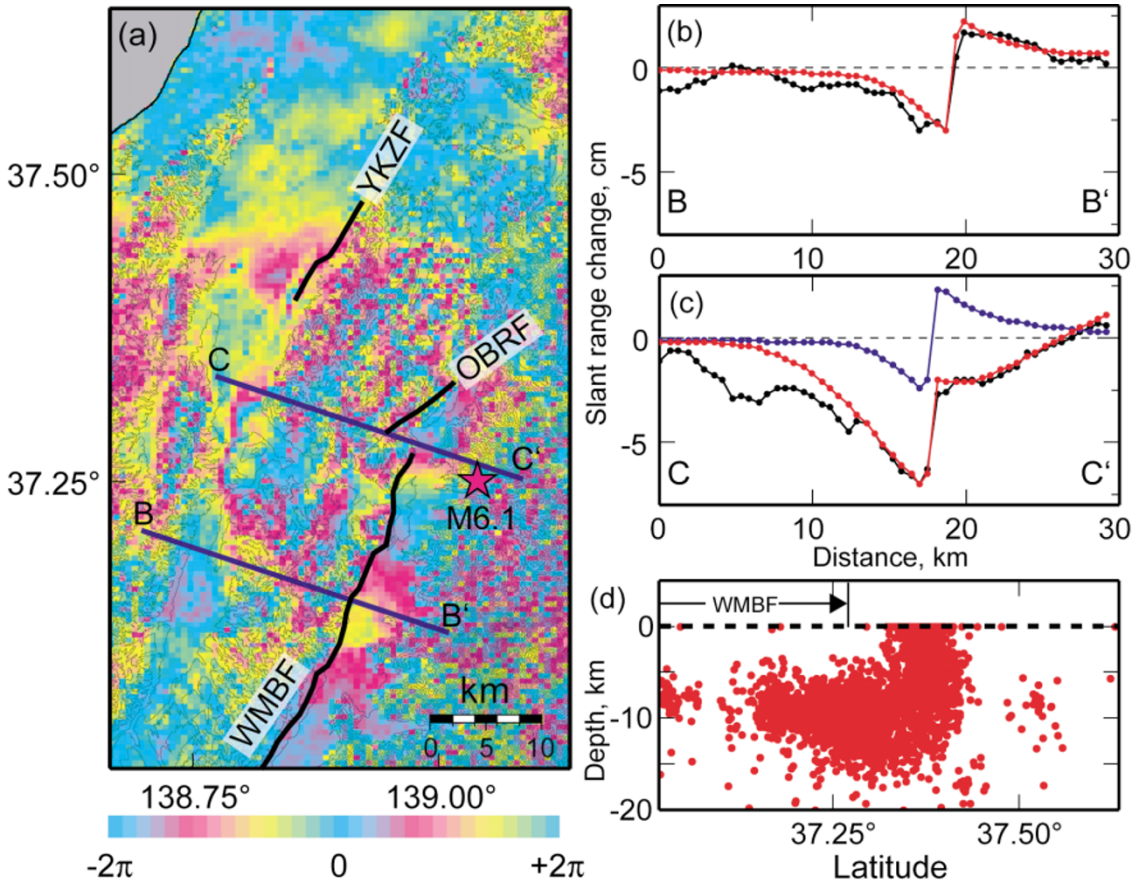

Fig. 3. (a) Interferogram generated from SAR data acquired on October 24 and November 17. Thick solid lines represent the Yukyuzan (YKZF), the Obiro (OBRF), and the Western Muikamachi Basin faults (WMBF). Purple star denotes the epicenter of the aftershock on October 27 (M6.1). Thin contours represent the topographic height every 100 m. The blue lines correspond to profiles BB′ and CC′ illustrated in Fig. 3(b) and (c). (b) Displacement profile along BB′ of Fig. 3(a). The solid and red curves denote observed and simulated displacements. (c) Displacement profile along CC′ of Fig. 3(a). The solid curve indicates the observed displacement. The blue curve represents the displacement profile simulated from a model supposing a single fault, which is consistent with the Obiro fault. The red curve represents the displacement profile simulated from a model supposing two faults, which is in the conjugate relation. (d) Distribution of aftershocks that occurred from October 24 to November 17, provided by JMA.

Table 3. Fault parameters estimated from the interferogram of the postseismic period.

Fault *1	Latitude*2 (°)	Longitude*2 (°)	Depth*2 (km)	Strike (°)	Dip (°)	Rake (°)	Length (km)	Width (km)	Slip (m)
A	37.168	138.871	5	205	60	90	18	5.8	0.06
B	37.321	138.945	5	205	60	90	12	5.8	0.06
C	37.276	139.065	16	25	30	90	12	15.0	0.38

*1 A, B, and C correspond to the Western Muikamachi Basin fault, the Obiro fault, and the fault of the aftershock on October 27.

*2 Indicates the location of the lower center of the fault.

27 ($M_{JMA} = 6.1$) must be included in the displacement field around this area. Based on the distribution of aftershocks, it has been suggested that this aftershock had ruptured a conjugate plane (e.g., Hirata *et al.*, 2005; Kato *et al.*, 2005; Sakai *et al.*, 2005; Shibutani *et al.*, 2005). We then tried to account for the displacement profile CC′ with the same method as in the previous section. The blue curve of Fig. 3(c) is the displacement profile simulated from a model supposing a single fault which is consistent with the Obiro fault. It hardly explains the observed displacement field. On the other hand, the red curve of Fig. 3(c) is the displacement profile simulated from a model supposing two faults, which is in the conjugate relation (Fault parameters were shown in B and C of Table 3). It explains the observed displacement field well, and therefore this deformation must have been caused by slips on two faults, the Obiro fault and the fault of the aftershock on October 27.

5. Summary

We applied RADARSAT SAR interferometry to detect crustal deformation associated with the Mid Niigata prefecture Earthquake in 2004. Fault parameters of the main

shock could be estimated from crustal deformation of the coseismic period, suggesting that the mechanism of the main shock might relate to a structure of a fold.

Crustal deformation in the postseismic period suggests that an aseismic slip occurred in the shallow part of the Western Muikamachi Basin fault. Additionally, crustal deformation associated with the aftershock on October 27 was detected, indicating that its aftershock had ruptured a conjugate plane with respect to the Obiro fault. These results demonstrate that at least three faults are related to this series of earthquakes, namely the main shock, the aftershock that occurred on October 27, and the Obiro-Western Muikamachi Basin faults. However, all of the observed crustal deformation cannot be explained by these faults, implying that other faults might also be involved in this series of earthquakes.

As mentioned in this paper, the mechanism of this series of earthquakes is very complex, and therefore more detailed investigations, combined with other data, will be required for future studies.

Acknowledgments. We would like to express our appreciation to Junko Nagai of ImageONE Co. Ltd., who worked hard on the acquisition request for RADARSAT SAR. The purchase of the RADARSAT SAR data was kindly supported by Shozo Matsumura. We are grateful to Naoshi Hirata and Shigeki Kobayashi for the useful review and suggestions. RADARSAT data was received by the Canadian Centre for Remote Sensing and distributed by RADARSAT International. SAR data was processed by SigmaSAR that was coded by Masanobu Shimada of the Japan Aerospace Exploration Agency. The hypocentral data was provided by the Japan Meteorological Agency in cooperation with the Ministry of Education, Culture, Sports, Science, and Technology. The coordinate data of GEONET was provided by the Geographical Survey Institute of Japan. All figures were drawn using the Generic Mapping Tools from Wessel and Smith (1998).

References

Hirata, N., H. Sato, S. Sakai, A. Kato, and E. Kurashimo, Fault system of the 2004 Mid Niigata prefecture earthquake and its aftershocks, *Landslides*, **2**(2), doi:10.1007/s10346-005-0050-8, 2005.

Imakiire, T., The result of crustal deformation observation related to the Mid Niigata Prefecture Earthquake, *Newsletter of Seism. Soc. Japan*, **16**, 29–33, 2005 (in Japanese).

Kato, A., E. Kurashimo, N. Hirata, S. Sakai, T. Iwasaki, and T. Kanazawa, Imaging the source region of the 2004 mid-Niigata prefecture earthquake and the evolution of a seismogenic thrust-related fold, *Geophys. Res. Lett.*, **32**, doi:10.1029/2005GL022366, 2005.

Maruyama, T., Y. Fusejima, T. Yoshioka, Y. Awata, and T. Matsu'ura, Characteristics of the surface rupture associated with the 2004 Mid Niigata Prefecture earthquake, central Japan and their seismotectonic implications, *Earth Planets Space*, 2005 (submitted).

Okada, Y., Surface deformation due to shear and tensile faults in a half-space, *Bull. Seism. Soc. Am.*, **75**, 1135–1154, 1985.

Sakai, S., N. Hirata, A. Kato, E. Kurashimo, T. Iwasaki, and T. Kanazawa, Multi-fault system of the 2004 Mid-Niigata Prefecture Earthquake and its aftershocks, *Earth Planets Space*, **57**, this issue, 417–422, 2005.

Samet, H. and R. E. Webber, Hierarchical data structures and algorithms for computer graphics. I. Fundamentals, *IEEE Comput. Graphics Appl.*, **2**(3), 48–68, 1988.

Shibutani, T., Y. Iio, S. Matsumoto, H. Katao, T. Matsushima, S. Ohmi, F. Takeuchi, K. Uehira, K. Nishigami, B. Enescu, I. Hirose, Y. Kano, Y. Kohno, M. Korenaga, Y. Mamada, M. Miyazawa, K. Tatsumi, T. Ueno, H. Wada, and Y. Yukutake, Aftershock distribution of the 2004 Mid Niigata Prefecture Earthquake, *Earth Planets Space*, 2005 (submitted).

Suzuki, Y., M. Watanabe, and D. Hirouchi, Report of the active fault research, http://www.seis.nagoya-u.ac.jp/INFO/niigata/reportAF1024.html, 2004 (in Japanese).

Wessel, P. and W. H. F. Smith, New, improved version of generic mapping tools released, *EOS Trans. AGU*, **79**(47), 579, 1998.

Yanagisawa, Y., I. Kobayashi, K. Takeuchi, M. Tateishi, K. Chihara, and H. Kato, Geology of the Ojiya district. With Geological Sheet Map at 1:50,000, *Geol. Surv. Japan*, 177 pp., 1986 (in Japanese with English abstract).

T. Ozawa (e-mail: taku@bosai.go.jp), S. Nishimura, Y. Wada, and H. Ohkura